Journal of Catalysis **206,** 1–13 (2002)
doi:10.1006/jcat.2001.3466, available online at http://www.idealibrary.com on IDEAL®

Pd-, Pt-, and Rh-Loaded $Ce_{0.6}Zr_{0.35}Y_{0.05}O_2$ Three-Way Catalysts: An Investigation on Performance and Redox Properties

H. He,*,†,[1] H. X. Dai,*,‡,[1] L. H. Ng,* K. W. Wong,§ and C. T. Au*,[1]

*Department of Chemistry, Hong Kong Baptist University, Kowloon Tong, Hong Kong; †College of Environmental and Energy Engineering, Beijing Polytechnic University, Beijing 100022, P.R. China; ‡Department of Applied Chemistry, Faculty of Science, Beijing University of Chemical Technology, Beijing 100029, P.R. China; and §Department of Physics, Chinese University of Hong Kong, Shatin, New Territories, Hong Kong

Received February 9, 2001; revised September 25, 2001; accepted October 23, 2001

The redox behaviors, oxygen mobilities, and oxygen storage capacities of $Ce_{0.6}Zr_{0.4}O_2$ (CZ), $Ce_{0.6}Zr_{0.35}Y_{0.05}O_2$ (CZY), and 0.5 wt% *M*/CZY (*M* = Pd, Pt, Rh) as well as the three-way catalytic performance of the noble metal-loaded CZY materials have been investigated. It is observed that at a space velocity of 60,000 h^{-1} and in an atmosphere close to the theoretical air-to-fuel ratio (i.e., 14.6), the CZY-supported precious metal catalysts showed good three-way catalytic activity. X-ray diffraction investigations revealed that there are two phases (cubic $Ce_{0.75}Zr_{0.25}O_2$, major; cubic $ZrO_{1.87}$, minor) in CZ, CZY, and 0.5 wt% *M*/CZY. These materials are porous and large in surface area. According to the results of Ce 3d X-ray photoelectron spectroscopic studies, the doping of Y^{3+} ions into the CZ lattice would cause the concentrations of oxygen vacancies and Ce^{3+} ions to increase. The results of H_2(or CO)–O_2 titration and temperature-programmed reduction–reoxidation experiments indicate the presence of a reversible redox behavior of Ce^{4+}/Ce^{3+} couples. The results of $^{18}O/^{16}O$ isotope exchange studies show that in the presence of oxygen vacancies and noble metals, the mobility of lattice oxygen on/in CZY is promoted. Based on the above outcomes, we suggest that by incorporating Y^{3+} ions into CZ and loading Pd, Pt, or Rh on CZY, one can enhance (i) lattice oxygen mobility, (ii) Ce^{3+} ion concentration, and (iii) oxygen uptake capacity of the CZY solid solution, generating a class of materials suitable for the catalytic conversion of automotive exhaust. © 2002 Elsevier Science (USA)

Key Words: **yttrium-incorporated CeO_2–ZrO_2 solid solutions; noble metal (Pd, Pt, Rh)-loaded $Ce_{0.6}Zr_{0.35}Y_{0.05}O_2$ catalysts; three-way exhaust catalysts; lattice oxygen mobility; oxygen storage capacity; $^{18}O/^{16}O$ isotope exchange.**

INTRODUCTION

In the past decades, environmental protection has become an increasing worldwide concern. Automobile exhaust is a major cause of air pollution. Three-way catalysts (TWC) which can eliminate CO, HC (hydrocarbons), and NO_x simultaneously have been used to control exhaust emissions. A conventional TWC usually contains noble metal(s) (Pd, Pt, and/or Rh), BaO, and CeO_2 as well as Al_2O_3. Recently, CeO_2 and related compounds have attracted much attention. Being facilitated by a facile Ce^{4+}/Ce^{3+} redox cycle, the materials exhibit a large oxygen storage capacity (OSC). They also show the abilities of (i) dispersing the noble metals, (ii) enhancing the thermal stabilization of the Al_2O_3 support, and (iii) promoting the water–gas shift reaction. Usually, a TWC shows good performance in the simultaneous elimination of CO, HC, and NO_x in lean and rich perturbations on each side of the stoichiometric air-to-fuel ratio (i.e., 14.6) (1). With an enhanced redox cycle of Ce^{4+}/Ce^{3+}, the catalytic performance of a TWC would be improved either in lean-burn or rich-burn atmospheres. A major drawback with these materials is CeO_2 sintering at high temperatures (e.g., ca. 800°C) (1). As a result, a large number of CeO_2-based binary oxides, such as CeO_2–Al_2O_3 (2), CeO_2–La_2O_3 (2), CeO_2–SiO_2 (3), CeO_2–HfO_2 (4), and CeO_2–ZrO_2 (5–13), have been investigated for thermal stability and OSC improvement.

Among these binary oxides, CeO_2–ZrO_2 was intensively studied for its good OSC and redox properties. The incorporation of ZrO_2 into the CeO_2 lattice yields a $Ce_xZr_{1-x}O_2$ solid solution with OSC and redox properties better than those of pure CeO_2. Working on a number of Rh-loaded $Ce_xZr_{1-x}O_2$ ($x = 0.1$–0.9), Graziani and coworkers (14, 15) found that the redox behaviors depend mainly on the composition and structure of the catalysts; the redox properties of a solid solution can be associated with the formation of oxygen vacancies as well as the activation energy for lattice oxygen mobility. Balducci *et al.* (15, 16) reported that the introduction of Zr into a CeO_2 lattice lowers the energy for Ce^{4+} reduction, and with the high mobility of lattice oxygen, the diffusion of oxygen from the bulk to the surface promotes the redox action of the Ce^{4+}/Ce^{3+} couples. A $Ce_xZr_{1-x}O_2$ solid solution can be in monoclinic, tetragonal, or cubic phase, depending on composition and method of preparation (17). Vidmar *et al.* (9) claimed that among the $Ce_xZr_{1-x}O_2$ solid solutions, the cubic one at $x = 0.4$ shows the best redox behavior and the largest OSC value. Doping a small amount of Y^{3+} into the $Ce_xZr_{1-x}O_2$ lattice

[1] To whom correspondence should be addressed. Fax: (852) 2339-7348. E-mail: pctau@hkbu.edu.hk.

0021-9517/02 $35.00

would result in an increase in OSC (9, 18), especially at a dopant level of $y = 0.025$ or 0.05 (in $Ce_{0.6}Zr_{0.4-y}Y_yO_2$) (18). In addition, the incorporation of Y^{3+} ions facilitates the diffusion of lattice oxygen by creating anion defects and thus decreases the temperature for the reduction of the solid solutions (18). Recently, Fally and coworkers pointed out that an improvement in OSC behavior of CeO_2–ZrO_2 (as compared to pure ceria) was independent of surface area (19), and the OSC enhancement that resulted in the incorporation of ZrO_2 in CeO_2 was not affected by a worsening of textural properties due to redox-aging (20). To our knowledge, there is no report on a combined investigation of redox properties, OSC, and catalytic performance of a Y_2O_3–CeO_2–ZrO_2 ternary solid solution with a noble metal loaded on it.

In this paper, we report the three-way catalytic performance of 0.5 wt% *M*/CZY (*M* = Pd, Pt, Rh; CZY = $Ce_{0.6}Zr_{0.35}Y_{0.05}O_2$); the reactant mixture was simulated to resemble an actual automotive exhaust. The redox properties and OSC of the materials were investigated by means of temperature-programmed reduction (TPR) and H_2–O_2 and CO–O_2 titrations. The oxygen mobility of $Ce_{0.6}Zr_{0.4}O_2$ (CZ), CZY, and *M*/CZY was probed using the $^{18}O/^{16}O$ isotope exchange method. We characterized these materials by means of techniques such as X-ray diffraction (XRD), and X-ray photoelectron spectroscopy (XPS).

EXPERIMENTAL

The CZ and CZY solid solutions were prepared by means of coprecipitation; (i) $Ce(NO_3)_3 \cdot 6H_2O$ (Aldrich, 99%) and $ZrO(NO_3)_2 \cdot xH_2O$ (Acros, 99.5%) for CZ and (ii) $Ce(NO_3)_3 \cdot 6H_2O$, $ZrO(NO_3)_2 \cdot xH_2O$, and Y_2O_3 (Acros, 99.99%; dissolved in dilute HNO_3) for CZY were mixed in an aqueous solution at the appropriate ratios. Then, an ammonia solution (3 N) was added dropwise to reach a pH value of about 10. The resulting precipitate was filtered, washed with distilled water, and dried in air at 80°C overnight. After calcination at 550°C in air for 5 h, the materials were cooled, ground, tableted, crushed, and sieved to a size range of 60–80 mesh.

To prepare the 0.5 wt% *M*/CZY catalysts, $RhCl_3 \cdot 3H_2O$ (Acros, 33 wt% Rh), $H_2PtCl_6 \cdot 6H_2O$ (Acros), and $PdCl_2$ (Acros, 59 wt% Pd) were dissolved in distilled water, and ammonia solution (3 N) was added dropwise for $M(OH)_x$ (*M* = Rh, Pt, and Pd) precipitation. The precipitates were filtered out and washed with dilute ammonia solution until there was no detection of Cl^- ions. The correct amount of $M(OH)_x$ was dissolved in dilute HNO_3 and *M* was loaded to CZY by means of wet impregnation. The resulted material was then dried at 80°C overnight followed by 5 h of calcination at 550°C.

The three-way catalytic activities were evaluated in a quartz tubular microreactor (i.d. = 10 mm) with the reactant mixture being simulated to resemble an actual automotive exhaust composition corresponding to an oxidants/reductants stoichiometric factor $\lambda = 1.00$; λ is defined as the molar ratio of $(2O_2 + NO)/(CO + 9C_3H_6)$. The concentrations of O_2, CO, C_3H_6, NO, H_2O, and CO_2 in the feedstock were 1.00%, 1.61%, 500 ppm, 1000 ppm, 10%, and 18%, respectively, with N_2 being the balance. The space velocity (SV) was 60,000 h^{-1}. The reaction temperature was regulated from 50–500°C at a rate of 3°C min^{-1} and monitored by means of a thermocouple located at the catalyst bed. We had 0.5 g of the catalyst well dispersed in 3 g of quartz sand and secured between two quartz wool plugs. Before the experiments, the sample was treated in a flow of reactants at room temperature for 0.5 h to eliminate the effect of reactant adsorption on the estimation of catalytic activities. The blank runs with only quartz sand and quartz wool plugs indicated that TWC activity was negligible below 550°C. The concentrations of CO, C_3H_6, and NO in the outlet of the reaction system were analyzed online with a nondispersive infrared analyzer (QGS-08B, BAIF), a flame ionization detector (NMH 45), and a Chemiluminescent $NO/NO_2/NO_x$ analyzer (Modal 8840, Monitor), respectively.

The TPR–reoxidation experiments were carried out in a similar kind of microreactor. For pretreatment, the sample (50 mg) was heated to 500°C in a flow of 50% O_2–50% N_2 (v/v, 50 ml min^{-1}) and maintained at this temperature for 1 h before being purged with N_2 at 500°C for 0.5 h. After TPR (from 25 to 950°C), the sample was reoxidized in a 50% O_2–50% N_2 mixture at 850°C for 1 h. The TPR–reoxidation cycle was repeated four times. The flow rate of the 5% H_2–95% N_2 (v/v) mixture for TPR was 50 ml min^{-1}. The effluent gases were monitored online by a thermal conductivity detector. The amount of H_2 consumed during the TPR process was quantified by calibrating the peak areas against that obtained when a known amount of CuO was reduced according to similar procedures.

For H_2–O_2 and CO–O_2 titrations, the experiments were performed in a quartz tubular microreactor (i.d. = 4 mm) by pulsing in O_2 and H_2 (or CO), alternately. The sample (50 mg) was placed in the middle of the reactor secured by two quartz wool plugs. A thermocouple located at the catalyst bed was used for temperature measurement. The size of each pulse was 50.0 μl. The effluent gases were monitored online with a mass spectrometer (HP G-1800A). Before H_2–O_2 and CO–O_2 titrations, the sample was treated in O_2 (30 ml min^{-1}) at a desired temperature for 1 h and purged with He (30 ml min^{-1}) for 0.5 h.

The $^{18}O/^{16}O$ isotope exchange experiments were for the investigation of lattice oxygen mobility in the solid solutions. A catalyst sample (0.2 g) was placed in a microreactor and was thermally treated in He (HKO > 99.995%, 20 ml min^{-1}) at a desired temperature for 0.5 h. Then $^{18}O_2$ (HKO, 95–98%) was pulsed onto the sample (He as carrier gas, 20 ml min^{-1}) at various temperatures and the composition

of the outlet gas was monitored with a mass spectrometer. The data were taken at the tenth pulse, where the reaction reached a steady state.

The crystal structure of the catalyst was determined by an X-ray diffractometer (D-MAX, Rigaku) operating at 40 kV and 200 mA using Cu $K\alpha$ radiation. The patterns recorded were referred to the powder diffraction files–1998 ICDD PDF Database for identification. The pore sizes and the surface areas of the catalysts were measured on a Nova 1200 apparatus.

The XPS (Phi Quantum 2000) technique was used for surface characterization of the catalysts, using monochromatic Al $K\alpha$ as the excitation source. XPS spectra were recorded on fresh, heated (treated in He at 500°C for 1 h), and reduced (treated in 5% H_2−95% N_2 at 300°C for 0.5 h followed by purging with He for 10 min) samples. After the respective treatments, the samples were mounted and transferred to the spectrometer in a transparent GLOVE BAG (Instruments for Research and Industry, USA) filled with He to avoid exposure to air. Finally, the samples were outgassed in a vacuum (10^{-5} Torr) for 0.5 h and then introduced into the analyzer chamber (3×10^{-9} Torr) for analysis. The C 1s line at 284.6 eV was taken as a reference for binding energy calibration.

RESULTS

Three-Way Catalytic Performance of 0.5 wt% M/CZY (M = Pd, Pt, Rh)

Figure 1 presents the catalytic activities of 0.5 wt% *M*/CZY as related to reaction temperature at $\lambda = 1.00$ and SV = 60,000 h^{-1}. Figure 1a shows that under the reaction conditions adopted, the 0.5 wt% *M*/CZY catalysts exhibited high activities for CO oxidation; we observed a light-off temperature as low as 60°C. With a rise in temperature to 100°C, CO conversion became 12, 5, and 23% over Pd/CZY, Pt/CZY, and Rh/CZY, respectively. The lowest temperature for 100% CO conversion was 300°C over Rh/CZY, 320°C over Pd/CZY, and 390°C over Pt/CZY. The catalytic activity for CO oxidation increased in the order 0.5 wt% Rh/CZY > 0.5 wt% Pd/CZY > 0.5 wt% Pt/CZY. The three catalysts also showed good activities for C_3H_6 oxidation (Fig. 1b). We observed C_3H_6 elimination at ca. 150°C. At 500°C, C_3H_6 conversions were 79.0, 85.0, and 78.6% over the Pd-, Pt-, and Rh-loaded CZY catalysts, respectively. The order of catalytic activity for C_3H_6 oxidation was 0.5 wt% Pt/CZY ≈ 0.5 wt% Rh/CZY > 0.5 wt% Pd/CZY. The catalytic performance of 0.5 wt% *M*/CZY in NO elimination is shown in Fig. 1c. At equal temperature, Pd/CZY and Rh/CZY showed similar NO conversions and were superior to Pt/CZY in performance. One can observe that at 200°C, NO conversions were 94.6, 59.1, and 100%, respectively, over Pd/CZY, Pt/CZY, and Rh/CZY. The N_2O selectivities were 63.2, 69.2, and 58.0% at 80°C over Pd/CZY, Pt/CZY, and Rh/CZY, respectively, and decreased with a rise in reaction temperature (Fig. 2). The catalytic performance for NO elimination followed a sequence of 0.5 wt% Rh/CZY ≈ 0.5 wt% Pd/CZY > 0.5 wt% Pt/CZY.

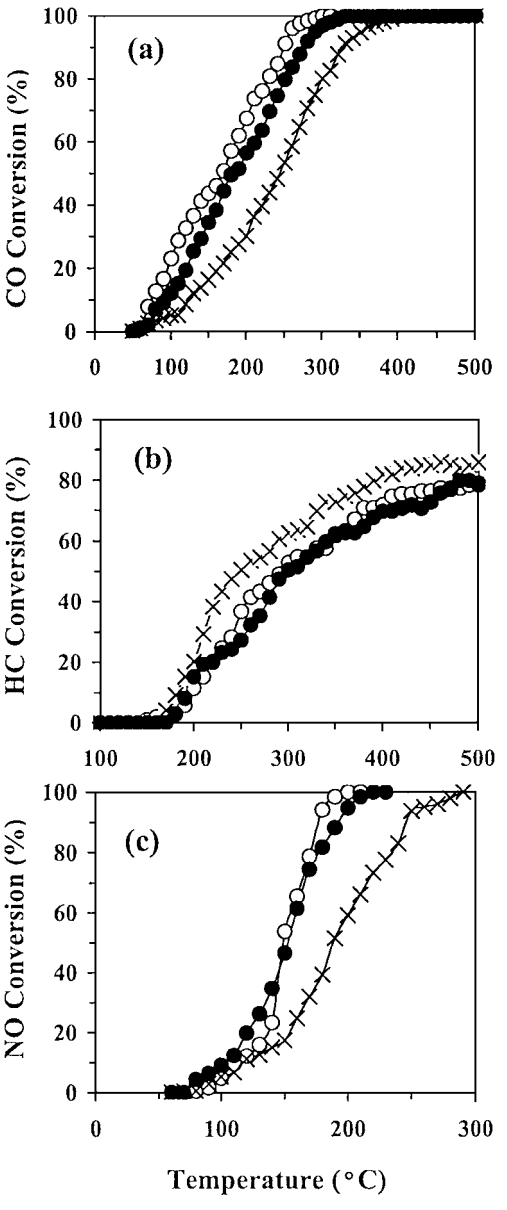

FIG. 1. (a) CO, (b) C_3H_6, and (c) NO conversions as related to reaction temperature over (●) 0.5 wt% Pd/CZY, (×) 0.5 wt% Pt/CZY, and (○) 0.5 wt% Rh/CZY.

Pore Structure, Surface Composition, BET, and XRD Studies

The surface composition and textural properties of CZ, CZY, and *M*/CZY are summarized in Table 1. The surface area of CZ was 52.9 $m^2\ g^{-1}$. The Ce/Zr atomic ratio (based on XPS results) on the surface of CZ was 0.34. The

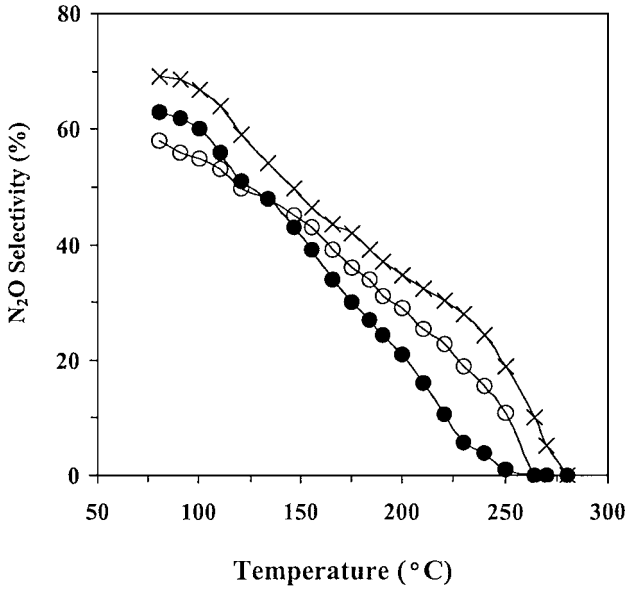

FIG. 2. N_2O selectivity as related to reaction temperature over (●) 0.5 wt% Pd/CZY, (×) 0.5 wt% Pt/CZY, and (○) 0.5 wt% Rh/CZY.

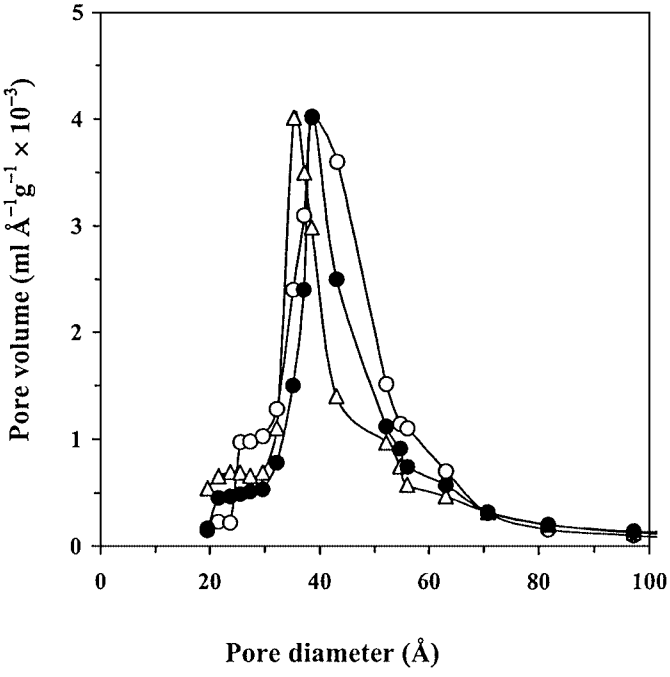

FIG. 3. Pore-size distributions of CZ (○), CZY (△), and 0.5 wt% Pd/CZY (●).

incorporation of Y^{3+} ions into the CZ lattice resulted in the generation of a CZY solid solution with surface area and Ce/Zr ratio equal to 69.1 $m^2\ g^{-1}$ and 0.78, respectively. The loading of 0.5 wt% Pd, Pt, or Rh on CZY caused a decrease in both surface area and Ce/Zr ratio. The pore-size distributions of CZ, CZY, and 0.5 wt% Pd/CZY are shown in Fig. 3. Since the profiles of pore-size distribution of Pt/CZY and Ph/CZY are similar to that of Pd/CZY, they are not shown here. The materials exhibited a narrow pore-size distribution (20–80 Å). The pore of CZY was more uniform in size than that of CZ. When a noble metal was loaded on CZY, the pore-size distribution became diffuse. The maximal pore volume was 4.01 ml g^{-1}at pore-size 38.3 Å for CZ, 4.02 ml g^{-1} at pore-size 35.2 Åfor CZY, and 4.01 ml g^{-1}at pore-size 38.0 Å for Pd/CZY. Above a pore size of 80 Å the pore volumes became very small. The average pore diameter was 63.5 Å for CZ and 48.7 Å for CZY. We observed that when 0.5 wt% Pd, Pt, or Rh was loaded on CZY, the pore size increased to ca. 58 Å.

Figure 4 shows the XRD patterns of fresh CZ, CZY, and 0.5 wt% *M*/CZY. Two phases, a major cubic $Ce_{0.75}Zr_{0.25}O_2$ (1998 ICDD PDF No. 28-0271) and a minor cubic $ZrO_{1.87}$ (1998 ICDD PDF No. 81-1551), were observed in all the samples. When Y^{3+} ions were introduced, the intensity of cubic $ZrO_{1.87}$ diffraction lines increased. The loading of a noble metal (Pd, Pt, or Rh) on CZY suppressed the formation of cubic $ZrO_{1.87}$. The XRD patterns (not shown here) of CZ, CZY, and *M*/CZY after H_2-TPR were similar to those of the corresponding fresh samples.

TPR–Reoxidation Cycle, H_2(CO)–O_2 Titration, and $^{18}O/^{16}O$ Isotope Exchange Studies

A good redox behavior and a strong oxygen storage ability would render a TWC well behaved under oscillatory reaction conditions. The TPR–reoxidation as well as the H_2–O_2 and CO–O_2 titration methods were adopted to

TABLE 1

Surface Area (*S*), Average Pore Diameter (*D*), Total Pore Volume (*V*), Surface Composition, and Ce/Zr Atomic Ratio

Catalyst	*S* ($m^2\ g^{-1}$)	*D* (Å)	*V* (ml g^{-1})	Surface composition (mol%)							Ce/Zr atomic ratio
				Pd	Pt	Rh	Ce	Zr	Y	O	
CZ	52.9	63.5	0.0671	—	—	—	5.02	14.6	—	80.3	0.34
CZY	69.1	48.7	0.0643	—	—	—	6.55	8.38	2.44	82.6	0.78
0.5 wt% Pd/CZY	36.3	59.0	0.0536	0.13	—	—	5.98	9.30	2.65	81.9	0.64
0.5 wt% Pt/CZY	37.8	57.9	0.0548	—	0.64	—	7.12	11.0	4.14	77.1	0.64
0.5 wt% Rh/CZY	36.9	57.5	0.0531	—	—	1.98	4.28	6.26	2.75	84.7	0.68

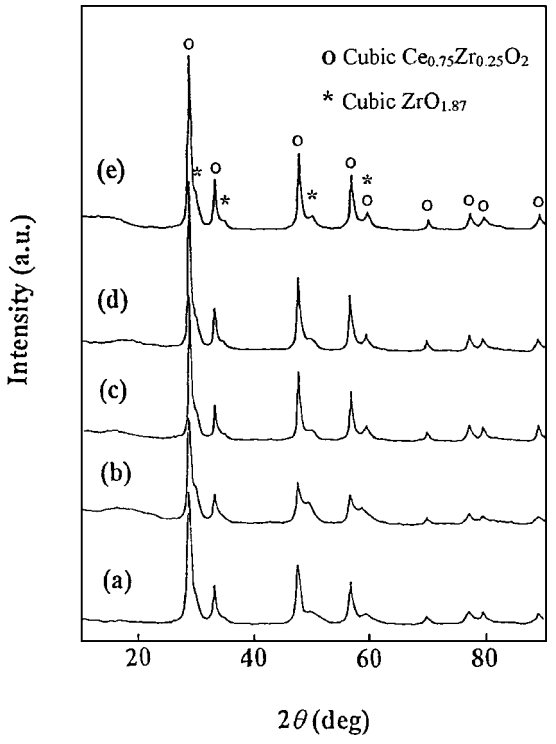

FIG. 4. XRD patterns of fresh (a) CZ, (b) CZY, (c) 0.5 wt% Pd/CZY, (d) 0.5 wt% Pt/CZY, and (e) 0.5 wt% Rh/CZY samples.

probe the redox behavior and oxygen storage capability of the catalysts. The TPR profiles of CZ and CZY are illustrated in Figs. 5 and 6, respectively. For a CZ sample in the first TPR–reoxidation cycle (Fig. 5a), there was a sharp reduction band at ca. 570°C with a shoulder centered at ca. 450°C and a broad band at ca. 850°C. As the TPR–reoxidation cycle was being repeated three times, the shoulder at ca. 450°C gradually disappeared and the reduction band at ca. 570°C shifted slightly to 600°C. For a CZY sample, there were two reduction bands at ca. 530 and 830°C in the first TPR run (Fig. 6a); the 530°C band split in two (at ca. 490 and 562°C) after the second cycle. Figure 7 shows the TPR profiles of the 0.5 wt% *M*/CZY catalysts; two reduction bands were observed in each case: at ca. 84 and 850°C over Pd/CZY; at ca. 245 and 830°C over Pt/CZY; and at ca. 110 and 810°C over Rh/CZY. With the loading of the metals, the reduction band at ca. 530°C observed over CZY (Fig. 6) vanished. Based on the amount of H_2 consumption observed over a standard CuO sample in similar TPR procedures, the amounts of reducible (by H_2) oxygen in CZ, CZY, and *M*/CZY were estimated and the data are summarized in Table 2. For the first TPR run, the amounts of reducible oxygen over CZ and CZY were 0.997 and 0.960 mmol g^{-1}. With the loading of 0.5 wt% Pt, Rh, and Pd on CZY, the amounts of reducible oxygen were 1.07, 1.05, and 0.840 mmol g^{-1}, respectively. After the samples were reoxidized in a 50% O_2–50% N_2 mixture at 850°C for 1 h, there were no significant changes in the amount of reducible oxygen in the CZ, CZY, 0.5 wt% Pt/CZY, and 0.5 wt% Rh/CZY samples, but there was a decrease over 0.5 wt% Pd/CZY (Table 2).

We conducted H_2–O_2 and CO–O_2 titration experiments to study further the redox behavior and oxygen storage ability of the samples and the results are summarized in Table 3. It can be observed that the O_2 uptakes as measured in H_2–O_2 and CO–O_2 titrations, as well as estimated according to the amounts of CO consumed and CO_2 produced in the CO–O_2 titration, were roughly the same, indicating that the data are reliable. In three consecutive cycles of the H_2–O_2 or CO–O_2 titration, the O_2 uptakes estimated according to O_2 consumption were rather similar, suggesting that the redox behavior is reversible.

In order to probe the oxygen mobility of the catalysts, we performed the $^{18}O/^{16}O$ isotope exchange experiments and the results are shown in Figs. 8 and 9. Over the catalysts, exchanges took place above ca. 400°C and increased with temperature rise. For the CZ catalyst at 550°C (Fig. 8a), the concentrations of $^{18}O_2$, $^{16}O_2$, and $^{18}O^{16}O$ were 82, 17, and 1.0%, respectively. With Y^{3+} incorporation into the CZ catalyst, $^{18}O/^{16}O$ exchange became significant; 61% $^{18}O_2$,

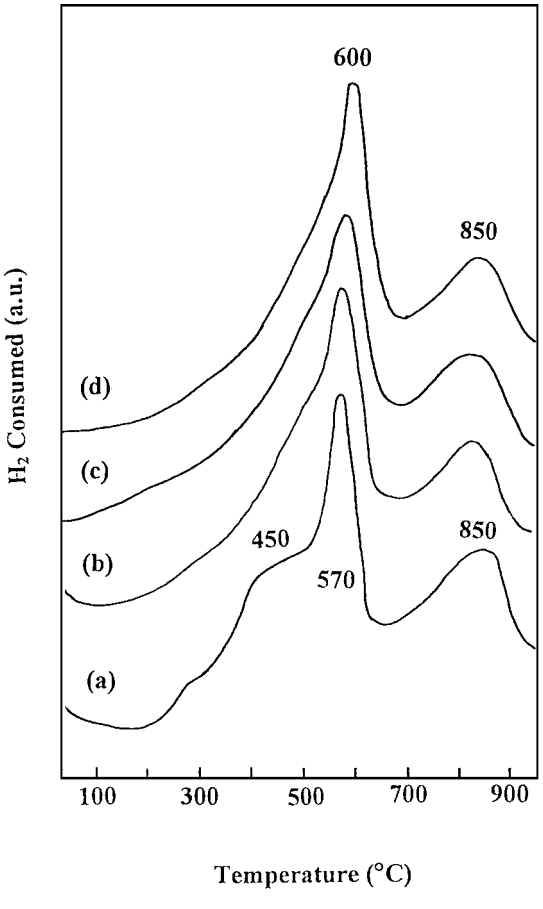

FIG. 5. TPR profiles of CZ: (a) Run 1, (b) Run 2, (c) Run 3, and (d) Run 4.

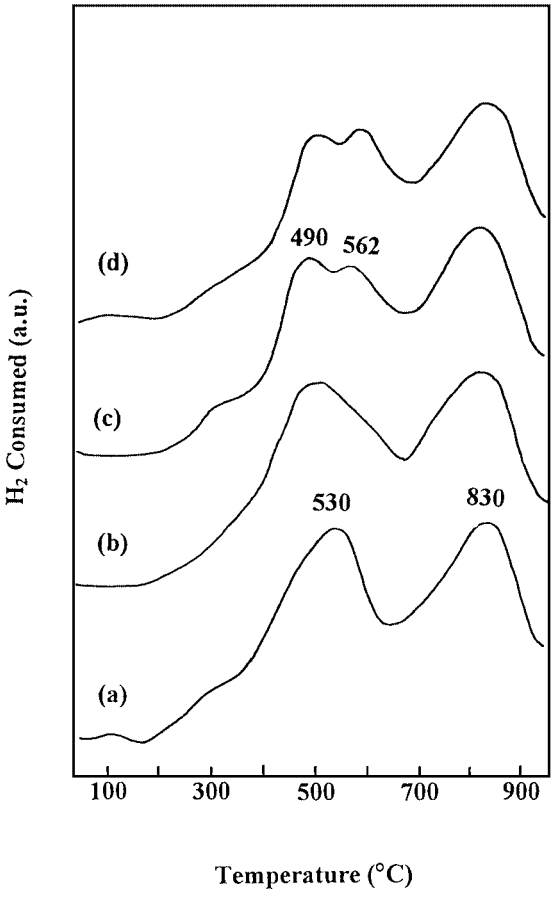

FIG. 6. TPR profiles of CZY: (a) Run 1, (b) Run 2, (c) Run 3, and (d) Run 4.

20% $^{16}O_2$, and 18.9% $^{18}O^{16}O$ were observed over the CZY catalyst at 550°C (Fig. 8b). Over 0.5 wt% Pd/CZY, the $^{18}O/^{16}O$ exchange was slightly undermined (Fig. 9a). However, the loading of 0.5 wt% Pt or 0.5 wt% Rh onto CZY enhanced the exchange (Figs. 9b and 9c).

XPS Studies

Figures 10 and 11 show the Ce 3d XPS spectra of the H_2-reduced and O_2-oxidized CZ and CZY samples. There are two sets of spin–orbit multiplets (u and v) corresponding to the $3d_{3/2}$ and $3d_{5/2}$ contributions; the Ce 3d spectrum contains three main $3d_{3/2}$ features at ca. 900.8 (u), 907.6 (u_2), and 916.7 eV (u_3) and three main $3d_{5/2}$ features at ca. 882.5 (v), 889.6 (v_2), and 898.5 (v_3) eV. The u_3 and v_3 features could be assigned to $3d^9\,4f^0$ photoemission final state, whereas the (v, v_2) and (u, u_2) doublets are attributed to the final states of strong $3d^9\,4f^2$ and $3d^9\,4f^1$ mixing. These states arise from the core hole potential in the final state and 4f hybridization in the initial state (21–24). The signals at 916.7 (u_3) and 898.5 (v_3) eV could be assigned to the contributions of Ce^{4+} $3d_{3/2}$ and Ce^{4+} $3d_{5/2}$, respectively. Those of Ce^{3+} $3d_{3/2}$ and Ce^{3+} $3d_{5/2}$ appear at 900.8 (u) and 882.5 (v) eV (25). The v and v_2 as well as u and u_2 features are shake-down signals due to charge transfer from ligand (O 2p) to metal (Ce 4f). As for states v_1 at 885.6 eV and u_1 at 903.3 eV, according to the assignment convention proposed by Burroughs *et al.* (26), they belong to unique photoelectron features from the Ce^{3+} state. The states v_2 at 889.6 eV and u_2 at 907.6 eV are features of that nature from the Ce^{4+} state. Similar Ce 3d XPS structures have been observed before over a $SrCl_2$-promoted CeO_2 catalyst (27). By quantifying the surface Ce^{3+} ions according to curve-fitted data, it is found that after treatment in H_2 at 300 and 650°C, there were 24.2 and 25.1% Ce^{3+} in CZ and 30.0 and 33.4% Ce^{3+} in CZY, respectively. As for the samples treated in O_2 at 300 and 500°C, there were 23.7 and 20.1% Ce^{3+} in CZ and 20.4 and 18.4% Ce^{3+} in CZY, respectively. The results indicate that the presence of Y^{3+} in the samples would promote the reduction of Ce^{4+} to Ce^{3+} in H_2 treatment and the oxidation of Ce^{3+} to Ce^{4+} in O_2 treatment.

DISCUSSION

Phase Composition and Surface Texture

There has been controversy over the nature of ceria–zirconia mixed oxides. Generally speaking, the mixed

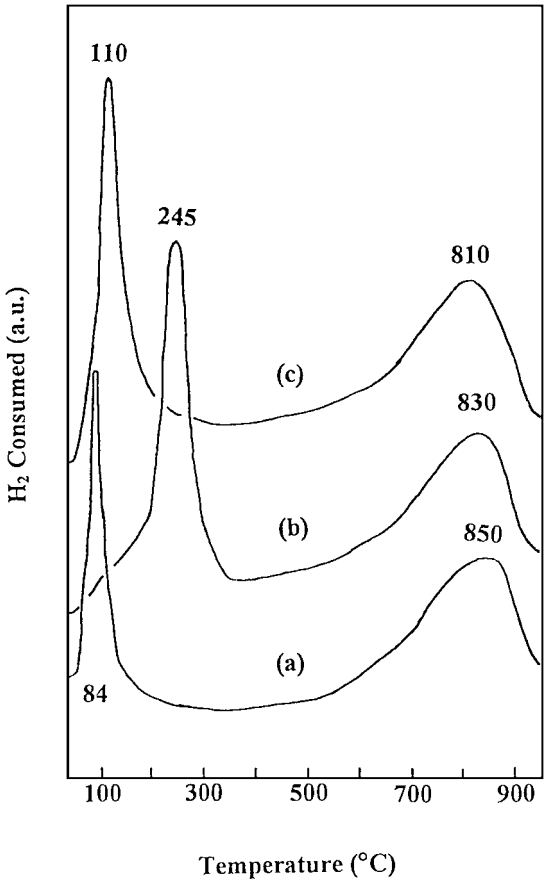

FIG. 7. TPR profiles of (a) 0.5 wt% Pd/CZY, (b) 0.5 wt% Pt/CZY, and (c) 0.5 wt% Rh/CZY.

TABLE 2

The Amount and Percentage of Reducible Oxygen in the Catalysts as Estimated According to H_2 Consumption in Four TPR Runs (R1 to R4) of TPR–Reoxidation Experiments

Catalyst	Amount of reducible oxygen (mmol g^{-1})				Percentage of reducible oxygen to total oxygen in catalysts (%)			
	R1	R2	R3	R4	R1	R2	R3	R4
CZ	0.997	0.951	0.870	0.818	14.2	13.6	12.4	11.6
CZY	0.960	0.941	0.980	1.02	13.7	13.4	14.1	14.7
0.5 wt% Pd/CZY	0.840	0.731	0.662	0.530	12.0	10.4	9.45	7.65
0.5 wt% Pt/CZY	1.07	1.08	0.970	0.960	15.3	15.6	14.0	13.8
0.5 wt% Rh/CZY	1.05	1.02	0.977	0.980	15.1	14.6	14.0	14.0

oxides are considered to be solid solutions. For example, Graziani and coworkers, and others, have reported three different tetragonal phases (t, t', and t'') and one cubic (c) phase in a CeO_2–ZrO_2 solid solution (9, 12, 28–30). Egami *et al.* suggested that there were actually mixed phases (a mixture of CeO_2 and cubic (Zr, Ce)O_2 in a CeO_2–ZrO_2 system (31)). It has been pointed out that the cubic phases are thermally more stable than the tetragonal phases (32, 33). The samples reported in the present study are composed of cubic $Ce_{0.75}Zr_{0.25}O_2$ and $ZrO_{1.87}$. When Y^{3+} was introduced into CeO_2–ZrO_2, the content of cubic $ZrO_{1.87}$ increased, implying the generation of additional oxygen vacancies. The particle sizes of $Ce_{0.75}Zr_{0.25}O_2$ in CZ and CZY were 7.50 and 6.62 nm, respectively. The results indicate that the distribution of Ce and Zr in the lattice was not homogeneous. They were nano-segregated into the Ce- and Zr-rich regions to produce different crystal grains. Egami *et al.* (31) proposed that there were exposed high-energy surfaces of CeO_2 at the grain boundaries from which oxygen atoms could be readily removed. Furthermore, the boundaries between the nanodomains might provide oxygen vacancies for easy oxygen passage. Similar situations would exist in our samples.

Recently, McCabe *et al.* (34) reported that the coexistence of several rare earth (Pr, La, and Nd) and alkaline earth (Ba and Ca) elements in CeO_2 exhibited a worsening effect on OSC behavior. We notice that ionic exchanges between phases were missing in these materials and there would be no generation of lattice defects. There are many reports on the generation of lattice defects upon the doping of rare earth and alkaline earth elements into CeO_2. For

TABLE 3

Oxygen Uptakes as Measured in H_2–O_2 and CO–O_2 Titrations at 450°C

Sample	O_2 uptake[a] (mmol g^{-1})			
	H_2–O_2 titration	CO–O_2 titration		
	(A)	A	B	C
CZ	0.38	0.31	0.36	0.32
CZY	0.52	0.50	0.52	0.50
0.5 wt% Pd/CZY	0.70	0.64	0.68	0.67
0.5 wt% Pt/CZY	0.60	0.54	0.55	0.56
0.5 wt% Rh/CZY	0.79	0.68	0.76	0.72

[a] Average of three cycles. A, Results based on O_2 consumption in O_2 pulsing. B, Results based on CO consumption in CO pulsing. C, Results based on CO_2 production in CO pulsing.

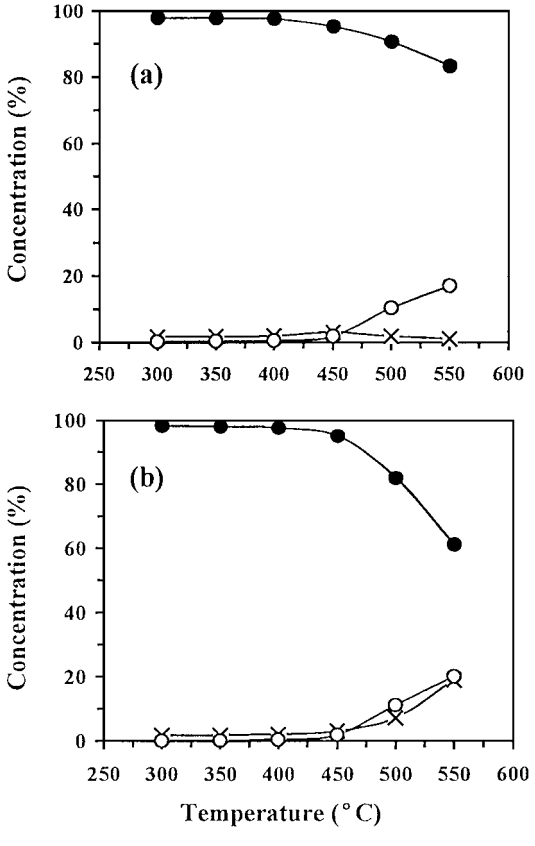

FIG. 8. $^{18}O/^{16}O$ isotope exchange over (a) CZ and (b) CZY. (●) $^{18}O_2$, (○) $^{16}O_2$, and (×) $^{18}O^{16}O$ concentrations.

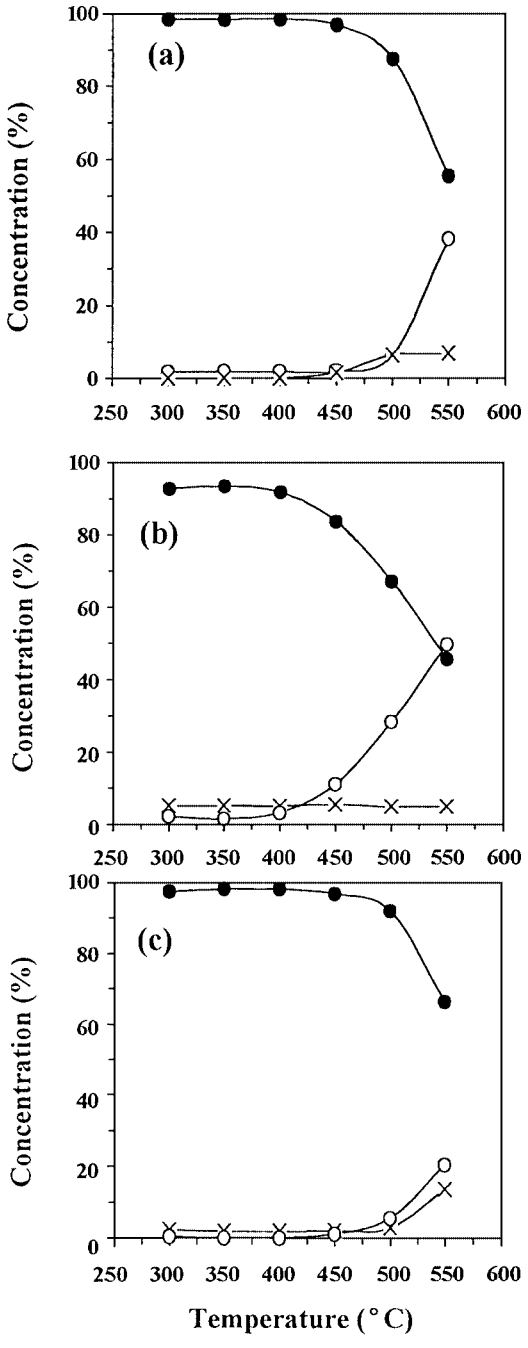

FIG. 9. $^{18}O/^{16}O$ exchange over (a) 0.5 wt% Pd/CZY, (b) 0.5 wt% Pt/CZY, and (c) 0.5 wt% Rh/CZY. (●) $^{18}O_2$, (○) $^{16}O_2$, and (×) $^{18}O^{16}O$ concentrations.

example, the partial dissolution of CaO in CeO_2 resulted in the generation of a fluorite-type CaO–CeO_2 solid solution that is superior in lattice oxygen mobility (35). It has been suggested that the incorporation of Ca^{2+} ions into a CeO_2 lattice would result in the generation of defect sites that promote the redox actions between Ce^{4+} and Ce^{3+} (36). The lattice oxygen in nanoscrystalline $Ce_xLa_{1-x}O_{2-y}$ is highly active, as the material could be reduced by H_2 at temperatures as low as 200°C (37). It is reported that with the incorporation of Zr^{4+} ions into CeO_2, the temperature for H_2-reduction decreased from ca. 850 to 670°C, suggesting that the CeO_2–ZrO_2 material released oxygen at a much lower temperature than did pure CeO_2 (38). Oxygen vacancies in the defective structures of CZY are believed to be responsible for the good performance observed in CO oxidation at low temperature (<100°C) (14, 29) and in NO removal (29), as well as for the high tendency of oxygen diffusion (14). Solid compounds of different textures usually show different redox, oxygen storage, and catalytic properties. Generally speaking, for a catalyst of redox action, it is desirable to be large in surface area, nanoscale in particle size, porous in structure, and high in the amount of oxygen vacancies. The CZ sample reported here is a nanoscale and porous (average pore diameter, 63.5 Å) material with a large surface area (52.9 $m^2\,g^{-1}$). The incorporation of Y^{3+} into the CZ lattice resulted in a decrease in average pore size and an increase in surface area (Table 1) but no change in crystal structure (Fig. 4). When 0.5 wt% Pd, Pt, or Rh was loaded on CZY, the surface area decreased, whereas a significant increase in pore sizes was found. We suggest that these could be a result of strong metal–CZY interaction.

For practical performance, a TWC should be able to stand a temperature as high as 1000°C. At such a high temperature, sintering of nanoparticles would occur. The works of Fally and coworkers (19, 20) suggest that the OSC behavior of CeO_2–ZrO_2 materials is independent of textural properties. The results in Table 2 indicate that there were only slight changes in the amount of reducible oxygen in the

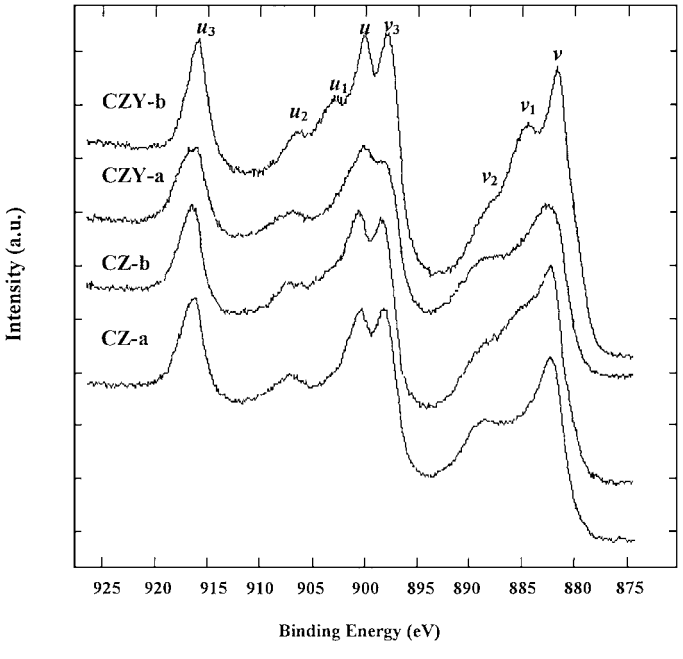

FIG. 10. Ce 3d XPS spectra of the CZ and CZY samples treated in H_2 at (a) 300 and (b) 650°C.

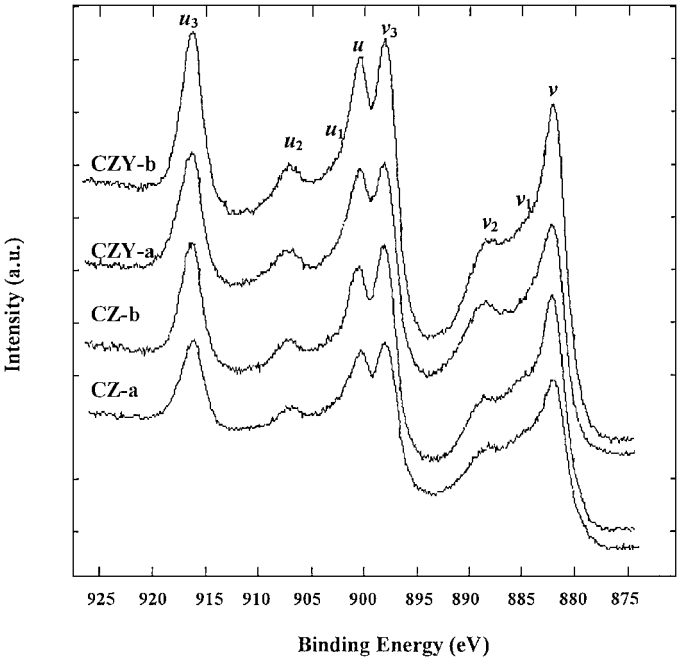

FIG. 11. Ce 3d XPS spectra of the CZ and CZY samples treated in O_2 at (a) 300 and (b) 500°C.

samples after cycles of TPR (25–950°C) and reoxidation (850°C). In other words, there was no obvious deterioration in oxygen mobility, OSC, or redox properties after various treatments at temperatures above 850°C. We deduce that the OSC behavior of these materials is also insensitive to changes in surface textures, such as sintering of nanoparticles and reduction in surface area.

Three-Way Catalytic Activities of the 0.5 wt% M/CZY Catalysts

CeO_2 is an important component because it acts as an oxygen buffer under the oscillatory operation conditions. The materials generated in the incorporation of ZrO_2 and Y_2O_3 into the lattice of CeO_2 reinforce the oxygen storage ability. In order to understand the interaction between the noble metal and the oxygen storage agent in TWCs, reactions such as CO and HC oxidation, NO reduction by CO and HC, and NO decomposition have been studied over CeO_2 and CeO_2–ZrO_2 loaded with noble metals. However, very few studies have been done on the actual three-way catalytic actions over these materials. Graziani and coworkers (7, 10, 30) pointed out that CeO_2–ZrO_2 loaded with noble metals showed good catalytic activities for NO decomposition and NO reduction by CO. Luo *et al.* (39) claimed that 5 wt% Pd/CeO_2 showed a light-off temperature (50% CO conversion) as low as 45°C. As shown in Fig. 1, the 0.5 wt% *M*/CZY catalysts showed good catalytic activities for CO oxidation and NO reduction. It has been reported that ZrO_2- and/or TiO_2-supported Au are good catalysts for CO oxidation at room temperature (40–52). Knell *et al.* (53) attributed the activity to the interaction of CO and surface OH^- and the oxidation of the resulted surface formate species by oxygen adatoms on the Au particles. To our knowledge, CO oxidation and NO reduction activities at such impressive levels have never been reported in actual automotive exhaust atmospheres.

When a CeO_2–ZrO_2 material is reduced in H_2 or CO, a certain amount of oxygen vacancies (V_o) would be generated, according to Eqs. [1] and [2]:

$$2Ce^{4+} + O^{2-} + H_2 \rightarrow 2Ce^{3+} + H_2O + V_o, \quad [1]$$

$$2Ce^{4+} + O^{2-} + CO \rightarrow 2Ce^{3+} + CO_2 + V_o. \quad [2]$$

The ionic radii of Ce^{4+}, Ce^{3+}, and Zr^{4+} are 0.97, 1.14, and 0.84 Å, respectively. The reduction of Ce^{4+} to Ce^{3+} causes the CZ lattice to expand, and there is a gradual decrease in the concentration of oxygen vacancies extended from the surface to the bulk. Such a gradient enables the lattice oxygen to diffuse from the bulk to the surface, promoting the oxidation of surface Ce^{3+} ions as a result. Due to the fact that compared to Ce^{4+} and Zr^{4+}, Y^{3+} is lower in oxidation state and larger in size, the incorporation of Y^{3+} into a CZ lattice would generate oxygen vacancies and hence promote the outward diffusion of lattice oxygen. The deduction is substantiated by the results of $^{18}O/^{16}O$ isotope exchange (Fig. 8) and H_2–O_2 and CO–O_2 titration (Table 3) experiments. The oxygen vacancies associated with the Ce^{3+} ions near the noble metal particles in CZ-supported catalysts have been proposed to be the active sites for NO activation (7, 10). Similar situations could have appeared during the three-way catalytic reactions over the 0.5 wt% *M*/CZY catalysts. For the simultaneous removal of NO and CO, we propose a mechanism of (i) NO dissociative adsorption on the noble metals (Eq. [3]), (ii) the generation of N_2 and N_2O from N and O adspecies (Eq. [4]), (iii) Ce^{3+} oxidation into Ce^{4+} (Eq. [5]), and (iv) Ce^{4+} reduction by CO (Eq. [2]).

$$NO^* \rightarrow N^* + O^*, \quad [3]$$

$$4N^* + O^* \rightarrow N_2 + N_2O + V_o, \quad [4]$$

$$Ce^{3+} + O^* \rightarrow Ce^{4+} + O^-, \quad [5]$$

where $*$ is the adsorption site. As a matter of fact, Eqs. [1]–[5] constitute a catalytic redox cycle. In the redox process, CO and NO were eliminated concurrently. Over the three *M*/CZY catalysts, the activity for C_3H_6 oxidation is not as intense as that for NO or CO elimination. Based on these results, we suggest that the good TWC performance of 0.5 wt% *M*/CZY is due to the combined presence of (i) oxygen vacancies, (ii) Ce^{4+}/Ce^{3+} redox couples, and (iii) noble metal.

Oxygen Mobility

It has been pointed out that oxygen mobility is an important factor to be considered in the catalysis of a TWC system (54). According to Novakova and coworkers (55, 56), there are three types of exchanges in $^{18}O/^{16}O$ interactions over an oxide surface: (i) homoexchange in the gas phase without appreciable participation of the oxygen in the oxide (Eq. [6]),

$$^{18}O_{2(g)} + {}^{16}O_{2(g)} \rightarrow 2{}^{18}O{}^{16}O_{(g)}; \quad [6]$$

(ii) single heteroexchange with the involvement of only one oxygen from the oxide surface (Eqs. [7] and [8]), possibly via the formation of a triatomic surface intermediate,

$$^{18}O{}^{18}O(g) + {}^{16}O(s) \rightarrow {}^{18}O{}^{16}O_{(g)} + {}^{18}O(s), \quad [7]$$

$$^{18}O{}^{16}O(g) + {}^{16}O(s) \rightarrow {}^{16}O{}^{16}O_{(g)} + {}^{18}O(s); \quad [8]$$

and (iii) multiple heteroexchange with the participation of two oxygen atoms from the oxide (Eqs. [9]–[11]),

$$^{18}O{}^{18}O_{(g)} + 2{}^{16}O_{(s)} \rightarrow {}^{16}O_{2(g)} + 2{}^{18}O_{(s)}, \quad [9]$$

$$^{18}O{}^{16}O_{(g)} + 2{}^{16}O_{(s)} \rightarrow {}^{16}O_{2(g)} + {}^{16}O_{(s)} + {}^{18}O_{(s)}, \quad [10]$$

$$^{18}O{}^{16}O_{(g)} + 2{}^{18}O_{(s)} \rightarrow {}^{18}O_{2(g)} + {}^{16}O_{(s)} + {}^{18}O_{(s)}. \quad [11]$$

Che and Tench (57, 58) and Cunningham *et al.* (59) suggested that there are two possible mechanisms for the multiple heteroexchange. One is isotope exchange via a four-atomic surface intermediate $[(O_4)^-_{ads}]$ and the other is "place-exchange" via the displacement of a preadsorbed oxygen molecule by an oxygen molecule from the gas phase.

In the $^{18}O/^{16}O$ exchange experiments, $^{18}O^{16}O$ were ca. 1.0 and 18.9%, respectively, over CZ and CZY (Fig. 8), implying that the exchange in the gas phase was negligible. The logic is that if exchange in the gas phase was dominant, the $^{18}O^{16}O$ concentration should be rather similar over the two samples. Martin and Duprez (54) detected roughly equal fractions of $^{18}O^{16}O$ and $^{16}O_2$ during $^{18}O/^{16}O$ exchanges over H_2-reduced CeO_2 and suggested that the exchange took place equally via the single and multiple exchange mechanisms. However, due to a failure in detecting the signals of $^{16}O^{18}O$ within the 450–650°C range, Cunningham *et al.* (60) proposed a place-exchange mechanism for oxygen isotope exchanges. Over the CZ and CZY samples in the present work, exchanges proceeded above 400°C. If there were oxygen vacancies on the surface, O_2 would adsorb dissociatively on the noble metal particles as well as at the oxygen vacancies of the oxide, resulting in an equal chance of exchange occurring via the single as via the multiple mechanisms, just as in the case of H_2-reduced CeO_2 (54). The mechanism for oxygen isotope exchange over the CZY solid solution would be rather similar since there is the formation of oxygen vacancies due to the incorporation of Y^{3+} into the CZ lattice. The deduction is confirmed by the fact that the concentrations of $^{18}O^{16}O$ and $^{16}O_2$ detected over CZY are rather similar (Fig. 8b). It is well-known that oxygen adspecies usually dwell at the oxygen vacancies on/in a solid oxide. The implication is also inferred from the rise in Ce^{3+} concentration after yttrium doping (Figs. 10 and 11) because if the number of oxygen vacancies remained unchanged, the Ce^{3+} concentration should decrease rather than increase. Therefore, it is reasonable to consider that there was an increase in oxygen vacancy density due to Y doping. Since the amount of oxygen vacancies in CZ is smaller than that in CZY, oxygen isotope exchange would follow the place-exchange mechanism. The fact that the amount of $^{16}O_2$ is higher than that of $^{18}O^{16}O$ (Fig. 8a) supports this viewpoint. Furthermore, a rise in oxygen vacancy density denotes an enhancement in oxygen mobility inside the CZY solid solution.

Over the 0.5 wt% *M*/CZY catalysts, oxygen isotope exchange could proceed via the migration of ^{18}O adatoms from the noble metal to the surface as well as to the lattice of the CZY solid solution (54), resulting in the formation of the $^{18}O^{16}O$ species. The product distributions at 550°C over CZY and 0.5 wt% Pd/CZY are rather similar (Fig. 9a), indicating that the chances of having oxygen exchange on Pd and on CZY are rather equal. Over 0.5 wt% Pt/CZY at 550°C, the extent of the exchange increased and $^{18}O^{16}O$ became the dominant species among the products (Fig. 9b), implying that the exchange occurred mainly on Pt. This result is in agreement with that reported by Martin and Duprez (54). Over 0.5 wt% Rh/CZY at 550°C, 46.6% $^{18}O_2$ was detected in the effluent gas and $^{16}O_2$ was the dominant product. We suggest that the adsorption and desorption were more facile on Rh than on Pd and Pt, and oxygen exchange occurred at the Rh/CZY interface. Among the exchanges over CZ, CZY, and 0.5 wt% *M*/CZY, that over 0.5 wt% Rh/CZY was the most significant, implying that oxygen mobility is best promoted by loading Rh to CZY. Soria *et al.* (61) pointed out that Rh could be incorporated into the CeO_2 lattice during calcination, an indication of a strong Rh–CeO_2 interaction. We suggest that Rh–CZY interaction is the strongest among the three *M*/CZY catalysts.

Oxygen Storage and Redox Behavior

As stated before, TWCs work efficiently only within the operation window around an A/F ratio of 14.6. The addition of an oxygen storage agent (such as CeO_2) is to enlarge the operation window and hence to achieve an optimal working efficiency under learn-burn and rich-burn conditions. Fornasiero *et al.* (11) reported that in a TPR–oxidation investigation over CeO_2, O_2 uptake was 0.50 mmol g^{-1} whereas over a $Ce_{0.5}Zr_{0.5}O_2$ solid solution, it was 0.52 mmol g^{-1}; apparently there was no significant enhancement in OSC after the incorporation of

ZrO_2 into CeO_2. However, after measuring the oxygen uptakes of CeO_2 and $Ce_xZr_{1-x}O_2$ ($x = 0.50$–0.68) at 400°C, Madier *et al.* (62) claimed that the oxygen uptakes (0.586–0.603 mmol g^{-1}) of the Zr-doped catalysts were much higher than that (0.126 mmol g^{-1}) of the undoped catalyst. As shown in Table 3, the incorporation of Y^{3+} into the CZ lattice increased the O_2 uptake by ca. 40%, whereas the loading of 0.5 wt% *M* on CZY increased the uptake by ca. 50% (compared to that of CZ). During the oxygen uptake process, there is the involvement of a redox cycle between Ce^{4+} and Ce^{3+}, and the oxygen vacancies generated in Y^{3+} incorporation facilitate the reduction of Ce^{4+} to Ce^{3+} and the oxidation of Ce^{3+} to Ce^{4+} (as revealed in XPS studies (Figs. 10 and 11)). Therefore, the enhancement in CZY oxygen uptake could be attributed to the generation of oxygen vacancies. The facile adsorption and spillover of CO and H_2 from the *M* particles to a CZY surface can facilitate the reduction of Ce^{4+} to Ce^{3+}, promoting the redox behavior and increasing the oxygen uptake capacity as a result. In a redox cycle between Ce^{4+} and Ce^{3+} at 450°C, there were 37.6, 52.7, 71.0, 60.9, and 80.2% (estimated according to the amounts of O_2 consumed in H_2–O_2 titration (Table 3)) of Ce^{4+} ions reduced to Ce^{3+}, respectively, over the CZ, CZY, 0.5 wt% Pd/CZY, 0.5 wt% Pt/CZY, and 0.5 wt% Rh/CZY samples. Therefore, after reduction, the chemical compositions of the samples should be $Ce^{4+}_{0.6-x}Ce^{3+}_xZr_{0.4}O_{2-0.5x}$, $Ce^{4+}_{0.6-x}Ce^{3+}_xZr_{0.35}Y_{0.05}O_{1.975-0.5x}$, and 0.5 wt% $M/Ce^{4+}_{0.6-x}Ce^{3+}_xZr_{0.35}Y_{0.05}O_{1.975-0.5x}$ ($x = 0.23$, 0.27, 0.38, 0.32, and 0.43 for CZ, CZY, 0.5 wt% Pd/CZY, 0.5 wt% Pt/CZY, and 0.5% wt% Rh/CZY, respectively). The concentration of oxygen vacancies created by incorporating Y^{3+} into the CZ lattice as well as during TPR processes decreases in the order of 0.5% wt% Rh/CZY > 0.5 wt% Pd/CZY > 0.5 wt% Pt/CZY, in good agreement with the catalytic activity for CO and NO elimination over these catalysts.

It is noteworthy that the OSC measured by means of H_2–O_2 and CO–O_2 titrations at a desired temperature corresponded well to the reduction extent of Ce^{4+} on the surface and in the bulk of the CZY and 0.5 wt% *M*/CZY samples (Table 3). At the first TPR run over CZ (Fig. 5), the presence of two reduction bands (at 570 and 850°C) with a shoulder (at 450°C) indicates that there are at least two types of Ce^{4+} located at different surroundings. The reduction band at 570°C and the shoulder at 450°C could be assigned to the reduction of Ce^{4+} located on the surface and/or subsurface of $Ce_{0.75}Zr_{0.25}O_2$, whereas the band at 850°C was due to the reduction of bulk Ce^{4+}. After the first run, the shoulder disappeared while the two bands were left unchanged. The disappearance of the shoulder peak might be due to a change in sample surface texture, a result of calcination. After the TPR–reoxidation cycles, there was no further change in TPR profile except that the 570°C band detected in the first cycle shifted to 600°C, suggesting that there was a slight reduction in oxygen mobility of the solid solution, in agreement with the results reported by Vidmar *et al.* (9).

The incorporation of Y^{3+} in the lattice of CZ led to the alternation of reduction behavior of CZ; comparing the TPR profiles of CZ and CZY, the first reduction band of CZY is broader and lower in temperature, possibly due to the presence of oxygen vacancies. As the TPR–reoxidation procedures were repeated, the reduction band at 530°C shifted to lower temperature and spilt into two overlapping bands with the band at ca. 830°C unchanged. A key aspect of the Ce^{4+}/Ce^{3+} redox process in CZY is the generation of oxygen vacancies via the formation of $[Ce^{3+}$–V_o–$Ce^{3+}]$ clusters (63). The results of TPR studies over the CZY sample (Fig. 6) indicate that there are two types of $[Ce^{3+}$–V_o–$Ce^{3+}]$ clusters generated during the TPR processes, one was created at 490°C and the other at 562°C. In other words, two types of oxygen vacancies existed in the CZY sample after the TPR treatments.

As Pd, Pt, or Rh (0.5 wt%) was loaded on the CZY, the reduction band at ca. 530°C observed over CZY disappeared, and the band at ca. 830°C remained largely unchanged; in addition, there was a sharp reduction band at low temperature (<250°C) over each of the *M*/CZY samples (Fig. 7). Similar results have been reported before and the reduction bands at low temperatures were assigned to the reduction of noble metal oxides (10, 14, 15). Over the Pd-, Pt-, and Rh-loaded CZY samples, the total amounts of oxygen reduced during the first TPR run were ca. 0.840, 1.07, and 1.05 mmol g^{-1} (Table 2), and the percentages of the reduced oxygen as reflected in the first band (Fig. 7) to the total amount of reduced oxygen were ca. 42, 51, and 52%, respectively. These values are too large to be reasonably attributed to the reduction of noble metal oxides, as the amount (0.5 wt%) of noble metals loaded was far too small. Therefore, we suggest that the presence of noble metals facilitates the adsorption and spillover of hydrogen from the *M* particles to the interface (and subsequently to the CZY bulk), resulting in Ce^{4+} reduction at the *M*/CZY interface at low temperature.

CONCLUSIONS

Over the 0.5 wt% *M*/CZY (M = Pd, Pt, Rh) catalysts under the conditions of $\lambda = 1.00$ and SV = 60,000 h^{-1}, the catalytic performance followed the order (i) Rh/CZY > Pd/CZY > Pt/CZY for CO oxidation, (ii) Pt/CZY > Rh/CZY ≈ Pd/CZY for C_3H_6 oxidation, and (iii) Rh/CZY ≈ Pd/CZY > Pt/CZY for NO elimination. The CZ and CZY as well as the *M*/CZY catalysts are composed of cubic $Ce_{0.75}Zr_{0.25}O_2$ and $ZrO_{1.87}$. The incorporation of Y^{3+} ions into the CZ lattice caused the oxygen vacancy density and the Ce^{3+}concentration to rise, as confirmed by the results of XPS studies. The H_2 (or CO)–O_2 titration and TPR–reoxidation results revealed that the redox between

Ce^{4+} and Ce^{3+} is reversible. The outcome of $^{18}O/^{16}O$ isotope exchange studies showed the promoting effects of oxygen vacancies and noble metals on the mobility of lattice oxygen. Hence, we conclude that (i) the inclusion of Y^{3+} ions in the CZ lattice enhances the formation of oxygen vacancies; (ii) the presence of oxygen vacancies as well as the loading of Pd, Pt, or Rh on CZY enhances the oxygen mobility and promotes the Ce^{4+}/Ce^{3+} redox cycle, as well as increases the oxygen uptake capacity of CZY; and (iii) the good three-way catalytic performance of 0.5 wt% *M*/CZY can be associated with the enhancements in oxygen vacancy concentration, redox behavior, oxygen mobility, and oxygen storage ability.

ACKNOWLEDGMENT

The work described in this paper was supported by a grant from the Hong Kong Baptist University (FRG/00-01/I-15).

REFERENCES

1. Farrauto, R. J., and Bartholomew, C. H., "Fundamentals of Industrial Catalytic Processes." Blackie Academic & Professional, London, 1997.
2. Usman, R. K., Graham, G. W., Watkins, W. L. H., and McCabe, R. W., *Catal. Lett.* **30**, 53 (1995).
3. Bensalem, A., Bozon Verduraz, F., Delamar, M., and Bugli, G., *Appl. Catal.* **121**, 81 (1995).
4. Zamar, F., Trovarelli, A., De Leitenburg, C., and Dolcetti, G., *J. Chem. Soc. Chem. Commum.* 965 (1995).
5. Vlaic, G., Di Monte, R., Fornasiero, P., Fonda, E. P., Kašpar, J., and Graziani, M., *J. Catal.* **183**, 378 (1999).
6. Hashimoto, K., Toukai, N., Hamada, R., and Imamura, S., *Catal. Lett.* **50**, 193 (1998).
7. Fornasiero, P., Rao, G. R., Kašpar, J., Erario, F. L., and Graziani, M., *J. Catal.* **175**, 269 (1998).
8. Masui, T., Peng, Y., Machida, K., and Adachi, G., *Chem. Mater.* **10**, 4005 (1998).
9. Vidmar, P., Fornasiero, P., Kašpar, J., Gubitosa, G., and Graziani, M., *J. Catal.* **171**, 160 (1997).
10. Rao, G. R., Fornasiero, P., Di Monte, R., Kašpar, J., Vlaic, G., Balducci, G., Meriani, S., Gubitosa, G., Cermona, A., and Graziani, M., *J. Catal.* **162**, 1 (1996).
11. Fornasiero, P., Balducci, G., Di Monte, R., Kašpar, J., Sergo, V., Gubitosa, G., Ferrero, A., and Graziani, M., *J. Catal.* **164**, 173 (1996).
12. Fornasiero, P., Di Monte, R., Rao, G. R., Kašpar, J., Meriani, S., Trovarelli, A., and Graziani, M., *J. Catal.* **154**, 168 (1995).
13. Rao, G. R., Kašpar, J., Meriani, S., Di Monte, R., and Graziani, M., *Catal. Lett.* **24**, 107 (1994).
14. Fornasiero, P., Di Monte, R., Rao, G. R., Kašpar, J., Meriani, S., Trovarelli, A., and Graziani, M., *J. Catal.* **151**, 168 (1995).
15. Balducci, G., Kašpar, J., Fornasiero, P., Graziani, M., and Saiful Islam, M., *J. Phys. Chem. B* **101**, 1750 (1997).
16. Balducci, G., Kašpar, J., Fornasiero, P., Graziani, M., and Saiful Islam, M., *J. Phys. Chem. B* **102**, 557 (1998).
17. Yashima, M., Hirose, T., Katano, S., and Suzuki, Y., *Phys. Rev. B* **51**, 8018 (1995).
18. Ozaki, T., Masui, T., Machida, K., Adachi, G., Sakata, T., and Mori, H., *Chem. Mater.* **12**, 643 (2000).
19. Fally, F., Perrichon, V., Vidal, H., Kašpar, J., Blanco, G., Pintado, J. M., Bernal, S., Colon, G., Daturi, M., and Lavalley, J. C., *Catal. Today* **59**, 373 (2000).
20. Vidal, H., Kašpar, J., Pijolat, M., Colon, G., Bernal, S., Cordón, A., Perrichon, V., and Fally, F., *Appl. Catal. B* **27**, 49 (2000).
21. Kulkarni, G. U., Rao, C. N. R., and Roberts, M. W., *J. Phys. Chem.* **99**, 3310 (1995).
22. Kotani, A., Mizuta, H., Jo, T., and Parlebas, J. C., *Solid State Commun.* **53**, 805 (1985).
23. Wuilloud, E., Delley, B., Schneider, W.-D., and Baer, Y., *Phys. Rev. Lett.* **53**, 202 (1984); **53**, 2519 (1984).
24. Jo, T., and Kotani, A., *Phys. Scr.* **35**, 570 (1987).
25. Tsunekawa, S., Fukuda, T., and Kasuya, A., *Surf. Sci.* **457**, L437 (2000).
26. Burroughs, P., Hamnett, A., Orchard, A. F., and Thornton, G., *J. Chem. Soc. Dalton Trans.* 1686 (1976).
27. Dai, H. X., Ng, C. F., and Au, C. T., *J. Catal.* **199**, 177 (2001).
28. Yashima, M., Morimoto, K., Ishizawa, N., and Yoshimura, M., *J. Am. Ceram. Soc.* **76**, 1745 (1993).
29. Fajardie, F., Tempère, J. F., Manoli, J. M., Touret, O., Blanchard, G., and Mariadassou, G. D., *J. Catal.* **179**, 469 (1998).
30. Rao, G. R., Kašpar, J., Meriani, S., Di Monte, R., and Graziani, M., *Catal. Lett.* **24**, 107 (1994).
31. Egami, T., Dmowski, W., and Brezny, R., *SAE* Paper No. 970461 (1997).
32. Markaryan, G. L., Ikryannikova, L. N., Muravieva, G. P., Turakulova, A. O., Kostyuk, B. G., Lunina, E. V., Lunin, V. V., and Zhilinskay, E., *Colloid. Surf. A* **151**, 435 (1999).
33. Ikryannikova, L. N., Aksenov, A. A., Markaryan, G. L., Muravieva, G. P., Kostyuk, B. G., Kharlanov, A. N., and Lunina, E. V., *Appl. Catal. A* **210**, 225 (2001).
34. McCabe, R. W., Jen, H.-W., Chun, W., Graham, G. W., Haack, L. P., Straccia, A., and Benson, D., *Appl. Catal. A* **184**, 265 (1999).
35. Zhang, Z. L., and Baerns, M., *J. Catal.* **135**, 317 (1992).
36. Trovarelli, A., De Leitenburg, C., and Dolcetti, G., *CHEMTECH* **27**, 32 (1997).
37. Trudeau, M. L., Tschöpe, A., and Ying, J. Y., *Surf. Interface Anal.* **23**, 219 (1995).
38. Narula, C. K., Haack, L. P., Chun, W., Jen, H.-W., and Graham, G. W., *J. Phys. Chem. B* **103**, 3634 (1999).
39. Luo, M. F., Hou, Z. Y., Yuan, X. X., and Zheng, X. M., *Catal. Lett.* **50**, 205 (1998).
40. Kozlov, A. I., Kozlova, A. P., Liu, H. C. and Iwasawa, Y., *Appl. Catal. A* **182**, 9 (1999).
41. Boccuzzi, F., Chiorino, A., Tsubota, S., and Haruta, M., *J. Phys. Chem.* **100**, 3625 (1996).
42. Bollinger, M. A., and Vannice, M. A., *Appl. Catal. B* **8**, 417 (1996).
43. Yuan, Y. Z., Kozlova, A. P., Asakura, K., Wan, H. L., Tsai, K. R., and Iwasawa, Y., *J. Catal.* **170**, 191 (1997).
44. Fukushima, K., Takaoka, G. H., Matsuo, J., and Yamada, I., *Jpn. J. Appl. Phys. Part 1* **36**, 813 (1997).
45. Iizuka, Y., Tode, T., Takao, T., Yatsu, K., Takeuchi, T., Tsubota, S., and Haruta, H., *J. Catal.* **187**, 50 (1999).
46. Valden, M., Pak, S., Lai, X., and Goodman, D. W., *Catal. Lett.* **56**, 7 (1998).
47. Grunwaldt, J. D., Maciejewski, M., Becker, O. S., Fabrizioli, P., and Baiker, A., *J. Catal.* **186**, 458 (1999).
48. Tsubota, S., Nakamura, T., Tanaka, K., and Haruta, M., *Catal. Lett.* **56**, 131 (1998).
49. Grunwaldt, J. D., Kiener, C., Wogerbauer, C., and Baiker, A., *J. Catal.* **181**, 223 (1999).
50. Grunwaldt, J. D., and Baiker, A., *J. Phys. Chem. B* **103**, 1002 (1999).
51. Park, E. D., and Lee, J. S., *J. Catal.* **186**, 1 (1999).

52. Bondzie, V. A., Parker, S. C., and Campbell, C. T., *Catal. Lett.* **63**, 143 (1999).
53. Knell, A., Barnickel, B., Baiker, A., and Wokaun, A., *J. Catal.* **137**, 306 (1992).
54. Martin, D., and Duprez, D., *J. Phys. Chem.* **100**, 9429 (1996).
55. Novakova, J., *Catal. Rev.* **4**, 77 (1970).
56. Klier, K., Novakova, J., and Jiru, P., *J. Catal.* **2**, 249 (1963).
57. Che, M., and Tench, J., *Adv. Catal.* **31**, 7 (1982).
58. Che, M., and Tench, J., *Adv. Catal.* **32**, 1 (1983).
59. Cunningham, J., Goold, E. L., and Fierro, J. L. G., *J. Chem. Soc. Faraday Trans.* **78**, 785 (1982).
60. Cunningham, J., Cullinane, D., Farrell, F., O'Driscoll, J. P., and Morris, M. A., *J. Mater. Chem.* **5**, 1027 (1995).
61. Soria, J., Martinez, A. A., and Conesa, J. C., *Vacuum* **43**, 437 (1992).
62. Madier, Y., Descorme, D., Le Govic, A. M., and Duprez, D., *J. Phys. Chem. B* **103**, 10999 (1999).
63. Balducci, G., Kašpar, J., Fornasiero, P., and Graziani, M., *J. Phys. Chem. B* **102**, 557 (1998).